Applied Ocean Research xxx (2011) xxx–xxx

Contents lists available at SciVerse ScienceDirect

Applied Ocean Research

journal homepage: www.elsevier.com/locate/apor

Focusing of surface waves by variable bathymetry

L.S. Griffiths, R. Porter*

School of Mathematics, University of Bristol, Bristol BS8 1TW, UK

ARTICLE INFO

Article history:
Received 31 January 2011
Received in revised form 17 August 2011
Accepted 17 August 2011
Available online xxx

Keywords:
Focusing
Water waves
Underwater lens
Arbitrary bathymetry
Mild slope equations

ABSTRACT

Scattering of a monochromatic train of surface gravity waves incident on a finite region of arbitrary three-dimensional smoothly varying bathymetry is considered in this paper. The full three-dimensional linear water wave theory is approximated by the depth-averaged modified mild-slope equations and a Greens function approach is used to derive domain a integral equation for the function relating to the unknown surface over the varying bed. A simple but robust and effective numerical scheme is described to approximate solutions to the integral equation. The method is applied to bathymetries which exhibit focusing in the high-frequency ray-theory limit and used to illustrate that focusing occurs at finite wavelengths where both refractive and diffractive effects are included. Specifically, examples of elliptical and bi-convex lens bathymetries are considered.

1. Introduction

The idea of focusing of surface waves by underwater lenses was first proposed by [17]. The basic concept is rather simple: oblique waves are refracted by changes in depth and so as a wave passes from a depth h_1 to a smaller depth h_2, say, the refractive index n determined by $n = k_2/k_1 > 1$ allows oblique waves to 'straighten out', where k_1 and k_2 are the wavenumbers for travelling waves determined by the linear dispersion relation $K \equiv \omega^2/g = k_i \tanh k_i h_i$, $i = 1, 2$ [17] and subsequent later work by these authors used this idea to consider the focusing of surface waves by lenses which comprised horizontal underwater plates forming a 'Fresnel lens' (the type used in lighthouses and overhead projectors for example) in plan form, although a conventional bi-convex lens would work equally well. Thus incoming waves passing across the lens are transformed into a circular wave which converges at the focal point of the lens (see, for example, [26] and references therein). Linear theory and, later, nonlinear theory which accounted for the large amplitudes that arise in the vicinty of the focal point, were used with success in predicting large amplification of waves at focal points and these methods compared favourably with experiments in [26]. The theory used in this early work assumed that the effect of the depth dependence was simply manifested in a change in wavenumber which resulted in a two-dimensional wave equation in which the depth dependence was removed. Later, a numerical method based on fully three-dimensional linear theory was used by [20] to explore focusing by Fresnel and bi-convex lens [10] have used a different mechanism for focusing surface waves. Using a large periodic array of vertical cylinders whose diameters are much smaller than the incident wavelength, they appealed to homogenisation theory to argue large arrays of cylinders alter the wavenumber to create refraction. Using over 600 cylinders arranged to form a bi-convex lens, they demonstrated using direct numerical methods that focusing did indeed occur as homogenisation theory predicted.

Ref. [13] used similar ideas to previous authors, again employing a submerged horizontal plate in the shape of a lens to refract waves. In plan form the lens had an elliptical-arc leading edge and a circular-arc trailing edge. Here, the authors were exploiting ray theoretical result that incoming parallel rays entering an elliptical domain with refractive index $n = 1/\epsilon$ where ϵ is the ellipticity are exactly focussed on the far focal point P of the ellipse. By placing the centre of curvature of the trailing edge circular-arc at P the incoming rays refracted by the leading elliptical edge will be focussed on P. Experiments performed by [13] showed that this idea worked as predicted.

In this work we also take advantage of the elliptical lens focusing used by [13] and consider focusing of waves by an elliptical sea mount. Specifically, we examine the refraction of waves in otherwise constant depth h_1 incident on an elliptical mound, with a plateau at depth $h_2 < h_1$. According to geometric ray theory high frequency surface waves will be refracted by an abrupt change in depth and focus above the far focal point of the elliptical plateau (see Section 2 for a description of this apparently little known result). Of course, the change in depth could be effected by having waves pass across a submerged elliptical plate. Such a problem was considered by [30] and though they do mention focusing of waves, it is evidently clear that they are unaware of the ray theory result of exact focusing.

* Corresponding author.
E-mail address: richard.porter@bristol.ac.uk (R. Porter).

0141-1187/$ – see front matter © 2011 Elsevier Ltd. All rights reserved.
doi:10.1016/j.apor.2011.08.004

When waves pass across raised bathymetry, refraction often results in amplification of waves behind the bathymetry and many papers have investigated this phenomenon. Three heavily cited papers in this area are due to [11,6,29] presumably because these papers include experimental data. In [11,29] amplification of waves by paraboidal and ellipsoidal shoals on a flat bed are considered [6] used a rotated ellipsoidal protrusion sitting on a linear sloping bed profile and produced numerical results based on mild slope equations, a ray theory approach showing the formation of a caustic behind the protrusion and experimental results. In none of these pieces of work consider geometries which predict perfect focusing under ray theory.

In this paper, we consider smoothly varying bathymetries motivated by the presence of perfect focusing as predicted by ray theory. A domain integral equation approach is developed to solve the problem based on the modified mild-slope equations (see, for example, [7]) which represent the three-dimensional fluid motion by two-dimensional depth-averaged equations based on the assumption that the gradient of the bed is small compared to the non-dimensional wavelength. It is perhaps worthy of note that the same assumption is used in a short-wavelength geometric optics approach to predict refraction over varying bathymetry, where ray paths are orthogonal to the phase lines $S(x, y)$ equals a constant where S satisfies the eikonal equation $S_x^2 + S_y^2 = k^2(x, y)$ and $k\tanh(kh(x, y)) = \omega^2/g$. See, for example, the description in [18]. The modified mild-slope approximation can be extended (e.g., [24,2]) to larger bed gradients and made increasingly accurate by the introduction of more vertical modes in the depth averaging procedure.

There is a difference in how rays bend when confronted with an abrupt change in depth and a gradual change in depth, though the final ray directions are the same. Hence the perfect focusing result described earlier and outlined in Section 2 for the vertically sided elliptical sea mount is lost once the change is depth is smoothed out. This is not an issue that we are overly concerned with as ray theory is introduced mainly for the purpose of motivation. Indeed, as we are concerned with surface gravity waves, the wavelengths considered here will be large enough that the defocusing effects of the gradual change in depth is probably not as important as the finite wavelength effect. Moreover, the formulation we propose allows for diffractive as well as refractive effects. Thus, in order to maximise the focusing of wave energy, we require a minimal amount of diffraction from the submerged bathymetry and this provides a secondary reason for the use of a smoothly varying bed.

In this problem we therefore consider bathymetries which rises gradually and smoothly from the open depth h_1 onto plateau of depth h_2. We will consider plateau of both elliptical and bi-convex lens shapes to demonstrate focusing effects. In Section 3 we describe the implementation of the mild-slope approximation to the fully three-dimensional problem and the formulation of domain integral equations from the reduced two-dimensional mild-slope equations using a Greens function approach, similar to that used in [23]. Section 4 outlines a simple but effective numerical discretisation method used to approximate solutions to the integral equations based on rectangular and circular based discretisations of the horizontal projection of the undulating bed. There are some similarities between our approach in this paper and the dual reciprocity boundary element method of [31] although our method appears much more straightforward both to formulate and implement numerically.

Finally, in Section 5, we produce a selection of graphical demonstrations of focusing of surface waves, illustrating focusing close to predictions from ray theory as the wavelength is decreased. In doing so, we indicate that an elliptical lens provides better focusing than the bi-convex lenses used previously by authors examining wave focusing. In addition, we assess the convergence of the numerical method and compare our results with the experimental results of [11,29].

2. Motivation: geometric ray theory

2.1. Elliptical lens

The following description can be found in [19]. Consider an elliptical domain with refractive index $n > 1$ and major axis $2a$, minor axis $2b$. Then the eccentricity is defined as $\epsilon = \sqrt{1 - b^2/a^2}$ and the focal points P and P' lie at $\pm a\epsilon$ (see Fig. 1). According to ray theory, a ray parallel to the major axis is incident on the ellipse, and makes an angle θ_i with the normal NN' to the boundary at O. The ray proceeds from O at an angle θ_r with respect to NN' where Snell's relates θ_i to θ_r by $\sin\theta_i/\sin\theta_r = n$. The ray intercepts the major axis at P and P' is the point at which a ray from P is reflected at O by the boundary onto the axis. Then $\angle ONP = \pi - \theta_i$ and by the sine rule $OP = nNP$. Also $\angle NOP' = \theta_r$ whilst $\angle ONP' = \theta_i$ and now the sine rule gives us $OP' = nNP'$. Adding these two results together gives $POP' = nPNP'$ and if this is to be independent of the point O, then we have P and P' at the focal points when we get $2a = n2a\epsilon$. In other words, we require $n = 1/\epsilon$.

When considering water waves in the short wavelength limit, a wave approaching the point O at which the elliptical boundary representing a change in depth is locally straight. By insisting that there is no change in the component of the wavenumber parallel to this boundary, we arrive at the relation $k_1 \sin\theta_i = k_2 \sin\theta_r$ where k_1 and k_2 are wavenumbers of propagating waves in depths h_1 and h_2 outside and inside the elliptical boundary. Thus in order to focus waves we require the relation

$$n = \frac{k_2}{k_1} = \frac{1}{\epsilon}, \tag{2.1}$$

to be satisfied. Hence, given the frequency ω, h_1 and h_2, we may use (2.1) to determine ϵ for focusing under the ray-theory limit.

2.2. Convex lens

The focal length, f, of a bi-convex lens is determined by the lensmakers' equation (see, for example, [9, p. 248, eqn. 6.2]),

$$\frac{1}{f} = (n-1)\left(\frac{2}{R} - \frac{(n-1)d}{nR^2}\right), \tag{2.2}$$

where n is determined by (2.1), d is the thickness of the lens from front to back and R is the radius of curvature of the lens.

3. Diffraction of waves by arbitrary three-dimensional bathymetry

3.1. Specification of the problem

The problem is described using Cartesian coordinates with the x and y axes lying in the mean free surface and z directed vertically upwards. The bed elevation is then given by $z = -h(x, y)$ where $h(x, y)$ is a continuous function with continuous derivatives over the varying part of the bathymetry, an arbitrary finite simply connected domain $(x, y) \in D$, and is such that $h(x, y) = h_1$, a constant, when $(x, y) \notin D$. Thus we require $h = h_1$ on $(x, y) \in \partial D$, the boundary of D, but can allow ∇h to be discontinuous across ∂D.

Under the usual assumption of linearised water wave theory, there exists a velocity potential given by $\Re\{(-\mathrm{i}g/\omega)\Phi(x, y, z)\,\mathrm{e}^{-\mathrm{i}\omega t}\}$ where a time-harmonic dependence of angular frequency ω has been imposed and g is gravitational acceleration. We seek the time-independent complex potential $\Phi(x, y, z)$ which satisfies

$$(\nabla^2 + \partial_{zz})\Phi = 0, \quad -h(x, y) \le z \le 0, -\infty < x, y < \infty, \tag{3.1}$$

Please cite this article in press as: Griffiths LS, Porter R. Focusing of surface waves by variable bathymetry. Applied Ocean Research (2011), doi:10.1016/j.apor.2011.08.004

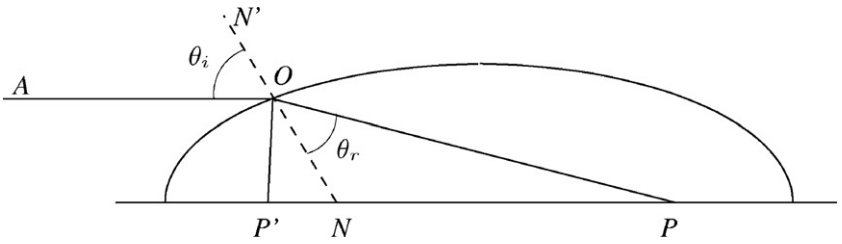

Fig. 1. Focusing of a ray on the far focal point of an ellipse.

where $\nabla = (\partial_x, \partial_y)$,

$$\Phi_z - K\Phi = 0, \quad \text{on } z = 0, \tag{3.2}$$

where $K = \omega^2/g$,

$$\Phi_z + \nabla h \cdot \nabla \Phi = 0, \quad \text{on } z = -h(x, y). \tag{3.3}$$

In addition Φ is required to satisfy a radiation condition at infinity which we set out to specify now. Outside the region $(x, y) \notin D$ where the bed is flat (3.3) reduces simply to the condition

$$\Phi_z = 0, \quad \text{on } z = -h_1 \text{ for } (x, y) \notin D, \tag{3.4}$$

and separable solutions may be sought. In particular, a wave of unit amplitude progressing from infinity over the flat bed and making an angle β with respect to the positive x-axis is given by the potential

$$\Phi_{inc}(x, y, z) = \frac{\cosh k_1(h_1 + z)}{\cosh k_1 h_1} e^{ik_1(x \cos\beta + y \sin\beta)}, \tag{3.5}$$

where we have written k_1 to denote the real, positive root of the usual linear dispersion relation

$$k_1 \tanh k_1 h_1 = K. \tag{3.6}$$

Since the governing equations are linear the total potential is written as the sum of the incident wave potential, Φ_{inc}, and a scattered wave potential, thus

$$\Phi(x, y, z) = \Phi_{inc}(x, y, z) + \Phi_{sc}(x, y, z), \tag{3.7}$$

where $\Phi_{sc}(x, y, z)$ results from the interaction of the incident wave with the undulating part of the bathymetry in $(x, y) \in D$ and must represent outgoing circular waves at large distances from this region. To be more precise, Φ_{sc} must satisfy the Sommerfeld radiation condition,

$$(k_1 r)^{1/2} \left(\frac{\partial}{\partial r} - ik_1 \right) \Phi_{sc} \sim o(1), \quad \text{as } k_1 r \to \infty, \tag{3.8}$$

where $r^2 = x^2 + y^2$ which implies

$$\Phi_{sc}(x, y, z) \sim \mathcal{A}(\theta; \beta) \left(\frac{2}{\pi k_1 r} \right)^{1/2} e^{i(k_1 r - \pi/4)} \frac{\cosh k_1(h_1 + z)}{\cosh k_1 h_1}, \quad k_1 r \to \infty. \tag{3.9}$$

Here $\mathcal{A}(\theta; \beta)$ is a measure of the scattered wave amplitude in the direction $\theta = \tan^{-1}(y/x)$ to the positive x-axis due to an incident wave propagating in the direction β.

3.2. The mild-slope approximation

The solution to the boundary-value problem specified above could, in principle, be approximated numerically by resorting to fully numerical methods, although these are computationally expensive and the application of the radiation condition is non-trivial.

We therefore seek to approximate its solution by invoking the mild-slope approximation. This has the effect of reducing the dimension of the problem by approximating the vertical structure of the velocity potential and averaging over the depth. Many versions of the mild-slope approximation have been (and continue to be) developed. Here, we use the modified mild-slope equations (MMSE) developed by [7] which extended the original mild-slope equations of [5,25] to include terms proportional to the bed gradient and curvature and which have been shown to produce more accurate results than previous models including the original MSE.

Thus we write

$$\Phi(x, y, z) \approx \frac{\cosh k(z + h)}{\cosh kh} \phi(x, y), \tag{3.10}$$

in which $k(h(x, y))$ denotes the positive, real root of the local dispersion relation

$$k \tanh kh = K, \tag{3.11}$$

where the depth is $h(x, y)$. In water of constant depth, for example when $h(x, y) = h_1$, $k(h(x, y))$ coincides with the definition k_1 seen in (3.6) and (3.10) is exact. Where $h(x, y)$ is varying, (3.10) is approximate in three different respects: Φ is not separable as (3.10) suggests; the vertical structure of fluid motion is treated as though only propagating waves are present; the form of the depth dependence implies that Φ locally satisfies a flat-bed condition and not a sloping-bed condition.

Variants of mild-slope approximations attempt to overcome one or more of these deficiencies but often at the cost of simplicity of the final equations. For example, the extended mild-slope equations (EMSE) derived by [24], expands Φ in a truncated series of depth eigenfunctions, thereby refining the vertical structure of the fluid flow. The couple-mode Mild-Slope Equations of [2] augment those depth eigenfunctions in the EMSE with a single extra 'bed mode' which also ensures that the sloping bed condition is satisfied exactly. Each of these developments lead to coupled systems of equations and add greatly to the complexity of the model.

A notable extension to the MMSE is the CMSE (the complementary MSE) introduced by [12] and a scalar version of this, the PMSE (pseudo-potential MSE), developed recently by [28]. Using the streamfunction to describe the flow-field, a single propagating mode with a separable depth dependence exactly satisfying the sloping bed condition is adopted. Thus, the simplicity of the original MSE/MMSE is retained whilst one of its approximations is overcome. Although PMSE can be used in the problems we consider in this paper to derive integral equations, the structure of the PMSEs leads to complications in the numerical approximation method and therefore we have adopted the MMSE here.

Though there are no formal bounds on the error incurred by various MSE models, the underlying assumption in each model is that $|\nabla h/kh| \ll 1$. Some analytical error estimates were produced by [22] for specific bed shapes.

Ref. [7] implemented the approximation (3.10) using a variational principle having (3.1)–(3.3) as its natural conditions, a procedure which replaces those equations by the single MMSE

$$\left.\begin{aligned} &\nabla \cdot (u_0 \nabla \phi) + v_0 \phi = 0, \quad -\infty < x, y < \infty, \\ &\text{with } v_0 = k^2 u_0(h) + u_1(h) \nabla^2 h + u_2(h) (\nabla h)^2. \end{aligned}\right\} \tag{3.12}$$

Please cite this article in press as: Griffiths LS, Porter R. Focusing of surface waves by variable bathymetry. Applied Ocean Research (2011), doi:10.1016/j.apor.2011.08.004

The positive-valued function $u_0(h(x,y))$ is given by

$$u_0 = \operatorname{sech}^2 kh(2kh + \sinh 2kh)/4k, \tag{3.13}$$

whilst the remaining coefficients in (3.12), u_1 and u_2, need not be given explicitly here, as they will shortly be subsumed into other terms. We remark, however, that (3.12) reduces to the original mild-slope equation of [5] if the terms u_1 and u_2 are discarded. A further simplification occurs in the long wave limit $kh \ll 1$ when (3.12) reduces to the familiar shallow water equation in which $u_0 = h$ and $v_0 = k^2 h = K$.

We note that use of (3.10) in the decomposition (3.7) implies

$$\phi(x,y) = \phi_{inc}(x,y) + \phi_{sc}(x,y), \tag{3.14}$$

where

$$\phi_{inc}(x,y) = \mathrm{e}^{\mathrm{i}k_1(x\cos\beta + y\sin\beta)}, \tag{3.15}$$

and

$$\phi_{sc}(x,y) \sim \mathcal{A}(\theta;\beta)\left(\frac{2}{\pi k_1 r}\right)^{1/2} \mathrm{e}^{\mathrm{i}(k_1 r - \pi/4)}, \quad \text{as } k_1 r \to \infty. \tag{3.16}$$

The function $\phi(x,y)$, which determines the approximation to Φ, is completely defined by (3.12)–(3.16).

We transform the equation (3.12) into its canonical form, by writing

$$\phi(x,y) = \left\{\frac{u_0(h_1)}{u_0(h(x,y))}\right\}^{1/2} \psi(x,y). \tag{3.17}$$

Then ψ satisfies

$$\nabla^2\psi + \kappa(x,y)\psi = 0, \quad -\infty < x, y < \infty, \tag{3.18}$$

where

$$\kappa(x,y) = k^2 + A(h)\nabla^2 h + B(h)(\nabla h)^2, \tag{3.19}$$

where $A(h(x,y))$ and $B(h(x,y))$, which include the functions u_1 and u_2 appearing in (3.12), are given by

$$A(h) = \frac{-2k}{P + \sinh P},$$
$$B(h) = k^2\{P^4 + 4P^3\sinh P + 3P^2(2\cosh^2 P + 1) + 18P\sinh P + 3\sinh^2 P(2\cosh P + 5)\}/\{3(P + \sinh P)^4\},$$

the abbreviation $P = 2kh$ having been used. Where there is a possible discontinuity in ∇h, allowed in our specification along the boundary ∂D of D, a direct integration of (3.18) across ∂D readily yields

$$[\mathbf{n}\cdot\nabla\psi]^+_- = -A(h_1)\psi[\mathbf{n}\cdot\nabla h]^+_- = A(h_1)\psi(\mathbf{n}\cdot\nabla h)_{\partial D^-} \tag{3.20}$$

(also see [22]) where $\mathbf{n}$ is the outward normal to the curve $(x,y) \in \partial D$ and the square brackets denotes the jump in the enclosed quantity from values on ∂D^+, exterior to D, to values on the interior, ∂D^-, of D. The final step in (3.20) is made from $\nabla h = 0$ for $(x,y) \notin D$ where $h = h_1$, a constant.

The 'flux' condition (3.20) is attributed to the $\nabla^2 h$ term and has used the fact that ψ, a proxy for the surface elevation (see (3.33)), must be continuous everywhere. The condition (3.20) appears to have been overlooked in other applications of the mild slope equations to numerical solutions of wave scattering over variable bathymetry which often include bathymetries with discontinuities in the bed slope, presumably in favour of the intuitive condition $[\mathbf{n}\cdot\nabla\psi]^+_- = 0$. For a recent example see [21].

Finally we mimic the decomposition of ϕ in (3.14) and write

$$\psi(x,y) = \psi_{inc}(x,y;\beta) + \psi_{sc}(x,y), \tag{3.21}$$

where

$$\psi_{inc}(x,y;\beta) = \mathrm{e}^{\mathrm{i}k_1(x\cos\beta + y\sin\beta)} = \mathrm{e}^{\mathrm{i}k_1 r\cos(\theta-\beta)}, \tag{3.22}$$

and

$$\psi_{sc}(x,y) \sim \mathcal{A}(\theta;\beta)\left(\frac{2}{\pi k_1 r}\right)^{1/2} \mathrm{e}^{\mathrm{i}(k_1 r - \pi/4)}, \quad k_1 r \to \infty. \tag{3.23}$$

3.3. Integral equation formulation

The boundary-value problem for ψ, (3.18)–(3.23) will be reformulated as an integral equation, making using of the fact that, for $(x,y) \notin D$, (3.18) reduces to the Helmholtz equation

$$(\nabla^2 + k_1^2)\psi = 0. \tag{3.24}$$

To carry this out we introduce the Greens function $G(x,y;x',y')$ defined by

$$(\nabla^2 + k_1^2)G = \delta(x-x')\delta(y-y'), \quad -\infty < x, y, x', y' < \infty, \tag{3.25}$$

and the radiation condition (3.8). The Greens function is simply given by

$$G(x,y;x',y') = -\frac{1}{4}\mathrm{i}H_0(k_1\rho) \tag{3.26}$$

(see for example, [18]) where $H_0(x) \equiv H_0^{(1)}(x) = J_0(x) + \mathrm{i}Y_0(x)$ is the Hankel function of the first kind and $\rho^2 = (x-x')^2 + (y-y')^2$. We make note of the behaviour

$$G(x,y;x',y') \sim -\frac{1}{4}\mathrm{i}\left(\frac{2}{\pi k_1\rho}\right)^{1/2} \mathrm{e}^{\mathrm{i}(k_1\rho - \pi/4)}, \quad \text{as } k_1\rho \to \infty, \tag{3.27}$$

and

$$G(x,y;x',y') \sim \frac{1}{2\pi}\ln(k_1\rho), \quad \text{as } k_1\rho \to 0, \tag{3.28}$$

which will be needed later.

To implement the solution process, we apply Green's Identity to $\psi_{sc}(x,y)$ and $G(x,y;x',y')$ over the whole (x,y)-plane by summing the contributions from separate applications in D and in $\mathbb{R}^2 \setminus D$, inside and outside the boundary ∂D to give

$$\begin{aligned}
&\int_{-\infty}^{\infty}\int_{-\infty}^{\infty}(\psi_{sc}\nabla^2 G - G\nabla^2\psi_{sc})\,\mathrm{d}x\,\mathrm{d}y \\
&= \lim_{\Gamma\to\infty}\int_0^{2\pi}\left(\psi_{sc}\frac{\partial G}{\partial r} - G\frac{\partial\psi_{sc}}{\partial r}\right)_{r=\Gamma}\Gamma\,\mathrm{d}\theta \\
&= \int_{\partial D}\left[\psi_{sc}\right]^+_-(\mathbf{n}\cdot\nabla G) - G\left[\mathbf{n}\cdot\nabla\psi_{sc}\right]^+_-\mathrm{d}s.
\end{aligned} \tag{3.29}$$

Using (3.18), (3.21), (3.23), (3.25), (3.20) and (3.27) in the above results in

$$\begin{aligned}
&\psi(x',y') + \iint_D [\kappa(x,y) - k_1^2]G(x,y;x',y')\psi(x,y)\,\mathrm{d}x\,\mathrm{d}y \\
&+ A(h_1)\int_{\partial D} G(x,y;x',y')\psi(x,y)(\mathbf{n}\cdot\nabla h)_{\partial D^-}\,\mathrm{d}s \\
&= \psi_{inc}(x',y';\beta),
\end{aligned} \tag{3.30}$$

for $-\infty < x', y' < \infty$.

Eq. (3.30), when restricted to $(x,y) \in D$, serves as an integral equation for the unknown reduced potential $\psi(x,y)$ on the domain D, whilst when applied to points $(x,y) \notin D$ allows the value of ψ to be computed in terms of those values solved for on $(x,y) \in D$. Notice that the incident wave angle, β, only appears in the right-hand side of (3.30), a fact that can lead to computational savings.

In order to determine the scattering amplitude $\mathcal{A}(\theta;\beta)$, we express the point (x',y') in the Greens function in terms of polar

Please cite this article in press as: Griffiths LS, Porter R. Focusing of surface waves by variable bathymetry. Applied Ocean Research (2011), doi:10.1016/j.apor.2011.08.004

coordinates (r', θ') located at the origin and find that

$$H_0(k_1\rho)\sim\left(\frac{2}{\pi k_1 r'}\right)^{1/2} e^{i(k_1 r'-\pi/4)}e^{-ik_1(x\cos\theta'+y\sin\theta')},$$
$$\text{as } k_1 r'\to\infty, \tag{3.31}$$

where $x' = r'\cos\theta'$ and $y' = r'\sin\theta'$. Using this and (3.26) in (3.30) and taking the limit as $k_1 r'\to\infty$ gives

$$\mathcal{A}(\theta';\beta) = \frac{1}{4}i\iint_D [\kappa(x,y)-k_1^2]\psi(x,y)\psi_{inc}(x,y;\pi+\theta')\,dx\,dy + \frac{1}{4}iA(h_1)\int_{\partial D}\psi(x,y)\psi_{inc}(x,y;\pi+\theta')(\mathbf{n}\cdot\nabla h)_{\partial D^-}\,ds. \tag{3.32}$$

The total free surface elevation due to an incident wave of unit amplitude is given by $\Re\{\eta(x,y)e^{-i\omega t}\}$, where

$$\eta(x,y) = \Phi(x,y,0) = \left\{\frac{u_0(h_1)}{u_0(h(x,y))}\right\}^{1/2}\psi(x,y), \tag{3.33}$$

and u_0 is given by (3.13).

Another quantity of interest is the total energy distributed in circular scattered waves to infinity. A measure of this quantity is defined to be

$$\mathcal{E} = \frac{1}{2\pi}\int_0^{2\pi}|\mathcal{A}(\theta;\beta)|^2\,d\theta. \tag{3.34}$$

It can be shown that $\mathcal{E} = -\Re\{\mathcal{A}(\beta;\beta)\}$ ([16]), a relation which in other physical contexts is known as the optical theorem.

The quantities $\mathcal{A}$ and $\mathcal{E}$ are most easily calculated by expanding ψ_{inc} in the (3.32) using the identity

$$\psi_{inc}(x,y;\beta) = e^{ik_1 r\cos(\theta-\beta)} = \sum_{n=-\infty}^{\infty} i^n J_n(k_1 r)e^{in(\theta-\beta)}. \tag{3.35}$$

Then (3.32) can be written as a Fourier series

$$\mathcal{A}(\theta';\beta) = \sum_{n=-\infty}^{\infty} A_n e^{in\theta'}, \tag{3.36}$$

where

$$A_n = \frac{1}{4}i^{1-n}\iint_D [\kappa(x,y)-k_1^2]J_n(kr)e^{-in\theta}\psi(x,y)\,dx\,dy + \frac{1}{4}i^{1-n}A(h_1)\int_{\partial D} J_n(kr)e^{-in\theta}\psi(x,y)(\mathbf{n}\cdot\nabla h)_{\partial D^-}\,ds, \tag{3.37}$$

and it follows that

$$\mathcal{E} = \sum_{n=-\infty}^{\infty}|A_n|^2 = -\Re\left\{\sum_{n=-\infty}^{\infty}A_n e^{in\beta}\right\}, \tag{3.38}$$

the second equation being on account of the optical theorem. The numerical scheme implemented in Section 4 to solve the integral equation satisfies this second equation in (3.38) exactly (to within machine precision) for any numerical discretisation; readers familiar with the properties of Galerkin's approximation to integral equations on such relations will not be surprised by this.

4. Numerical solution

The use of bathymetry with discontinuous bed slopes at the connection between the undulating part of the bed and the constant depth gives rise to line integrals in the formulation, see (3.30), (3.32) and (3.37). The aims of this paper, which concentrates on focusing of waves by bathymetry with large raised plateaus, can be achieved by assuming bathymetry which connects smoothly with the constant depth, thus avoiding an unnecessary complication to the numerical solution method. Therefore we restrict ourselves henceforth to cases where $(\mathbf{n}\cdot\nabla h)_{\partial D^-} = 0$ with one minor exception outlined later in Section 5.

4.1. Solution based on a rectangular domain

The simplest case to consider is when the undulating part of the bed, D, is confined within the boundaries of a rectangular domain $D_{ab} = \{|x|\le a, |y|\le b\}$. Since $\kappa = k_1^2$ in $D_{ab}\setminus D$, (3.30) and (3.32) hold with D replaced by the larger domain D_{ab}.

We make an approximation to the unknown $\psi(x,y)$, writing

$$\psi(x,y)\approx\sum_{i=1}^{N}\sum_{j=1}^{M}a_{ij}\psi_{ij}(x,y), \tag{4.1}$$

where a_{ij} are undetermined coefficients,

$$\psi_{ij}(x,y) = \begin{cases}1, & (x,y)\in D_{ij},\\ 0, & \text{otherwise},\end{cases} \tag{4.2}$$

are discrete step basis functions, and $D_{ij} = \{|x-x_i|<(1/2)\Delta_x, |y-y_j|<(1/2)\Delta_y\}$, with

$$\begin{cases} x_i = -a+\left(i-\frac{1}{2}\right)\Delta_x, \quad i=1,\dots,N,\ \Delta_x = \frac{2a}{N},\\ y_j = -b+\left(j-\frac{1}{2}\right)\Delta_x, \quad j=1,\dots,M,\ \Delta_y = \frac{2b}{M}.\end{cases} \tag{4.3}$$

Before using this approximation, we decompose G into singular and bounded components with $G = G_s + G_b$ where

$$G_b(x,y;x',y') = -\frac{i}{4}H_0(k_1\rho)-\frac{1}{2\pi}\ln(k_1\rho)\sim -\frac{i}{4} + \frac{1}{2\pi}(\gamma-\ln 2), \quad \text{as } k_1\rho\to 0, \tag{4.4}$$

Ref. [1], where $\gamma = 0.5772\ldots$ is Euler's constant and $G_s(x,y;x',y') = (2\pi)^{-1}\ln(k_1\rho)$. Inserting (4.2) into (3.30) approximates (3.30) by

$$\psi(x',y')+\sum_{i=1}^{N}\sum_{j=1}^{M}a_{ij}[\kappa(x_i,y_j)-k_1^2]\{\Delta_x\Delta_y G_b(x_i,y_j;x',y') + G_{ij}^s(x',y')\} = \psi_{inc}(x',y';\beta), \tag{4.5}$$

in which the integral involving the smooth part of the Greens function, G_b, has been approximated by a simple mid-point rule, and where the integral of the singular part is carried out exactly to give

$$G_{ij}^s(x',y') = \iint_{D_{ij}} G_s(x,y;x',y')\,dx\,dy = \frac{1}{4\pi}\left[\left[xy(\ln(k_1^2(x^2+y^2))-3)+x^2\tan^{-1}\left(\frac{y}{x}\right) + y^2\tan^{-1}\left(\frac{x}{y}\right)\right]_{x_i-x'-(1/2)\Delta_x}^{x_i-x'+(1/2)\Delta_x}\right]_{y_j-y'-(1/2)\Delta_y}^{y_j-y'+(1/2)\Delta_y}. \tag{4.6}$$

Here, $G_{ij}^s(x',y')$ is a smooth function of (x',y') over the whole domain. Hence, multiplying (4.5) by $\psi_{pq}(x',y')$ and integrating over D_{ab}(a

Please cite this article in press as: Griffiths LS, Porter R. Focusing of surface waves by variable bathymetry. Applied Ocean Research (2011), doi:10.1016/j.apor.2011.08.004

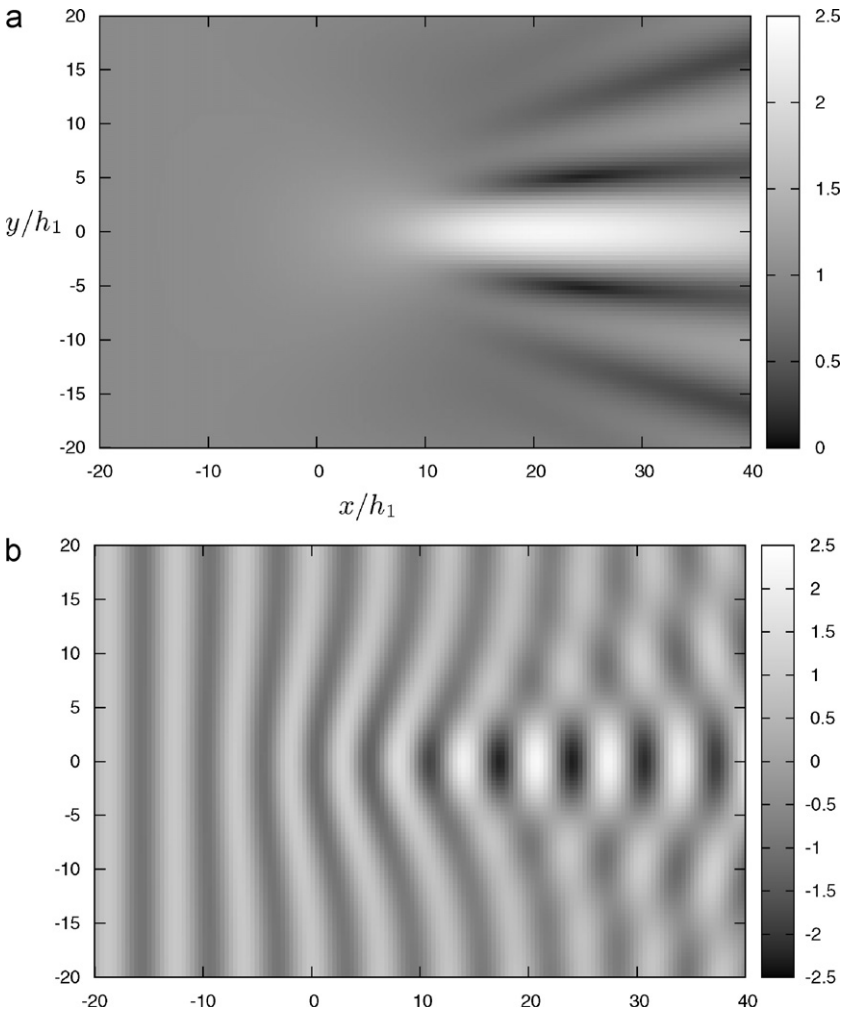

Fig. 2. Free surface displacement: (a) maximum over a period and (b) instantaneous for double-cosine bed defined by (5.1) with $a/h_1 = b/h_1 = 20$, $h_{max}/h_1 = 1/2$, $k_1 h_1 = 1$, $\beta = 0$.

process which characterises the Galerkin method) and approximating integrals by the mid-point rule gives

$$a_{pq} + \sum_{i=1}^{N}\sum_{j=1}^{M} a_{ij}[\kappa(x_i, y_j) - k_1^2]\{\Delta_x \Delta_y G_b(x_i, y_j; x_p, y_q) + G_{ij}^s(x_p, y_q)\} = \psi_{inc}(x_p, y_q; \beta), \tag{4.7}$$

for $p = 1, \ldots, N$, $q = 1, \ldots, M$. The solution to the system of equations (4.7) can be used to reconstruct ψ using (4.5), and hence the free surface using (3.33). The scattered wave amplitude, on substitution of (4.1) into (3.32), is approximated by

$$\mathcal{A}(\theta'; \beta) = \frac{1}{4}\mathrm{i}\Delta_x \Delta_y \sum_{i=1}^{N}\sum_{j=1}^{M} a_{ij}[\kappa(x_i, y_j) - k_1^2]\psi_{inc}(x_i, y_j; \pi + \theta'), \tag{4.8}$$

whose Fourier coefficients, defined by (3.36), are given by

$$A_n = \frac{1}{4}\mathrm{i}^{1-n}\Delta_x \Delta_y \sum_{i=1}^{N}\sum_{j=1}^{M} a_{ij}[\kappa(x_i, y_j) - k_1^2]J_n(kr_{ij})\,\mathrm{e}^{-\mathrm{i}n\theta_{ij}}, \tag{4.9}$$

with $r_{ij} = (x_i^2 + y_j^2)^{1/2}$, $\tan\theta_{ij} = y_j/x_i$.

We note finally that the approximation (4.1) with (4.2) and the evaluation of integrals be a mid-point rule whilst being simple to implement is crude and could most certainly be improved upon. However, the results converge quickly enough for our purposes as we shall see.

4.2. Solution based on a circular domain

If D is more closely aligned to a circular domain, it may be more effective to discretise the integral equation over D_b, a circular domain of radius b. The steps outlined above for the approximation and numerical solution follow in a similar fashion. We change the independent variables from (x, y) to (r, θ) and write

$$\psi(r, \theta) = \sum_{i=1}^{N}\sum_{j=1}^{M} a_{ij}\psi_{ij}(r, \theta), \tag{4.10}$$

where

$$\psi_{ij}(r, \theta) = \begin{cases} 1, & (r, \theta) \in D_{ij} \\ 0, & \text{otherwise,} \end{cases} \tag{4.11}$$

and now $D_{ij} = \{|r - r_i| < (1/2)\Delta_r, |\theta - \theta_j| < (1/2)\Delta_\theta\}$ with

$$\begin{cases} r_i = \left(i - \dfrac{1}{2}\right)\Delta_r, & i = 1, \ldots, N, \quad \Delta_r = \dfrac{b}{N}, \\ \theta_j = \left(j - \dfrac{1}{2}\right)\Delta_\theta, & j = 1, \ldots, M, \quad \Delta_\theta = \dfrac{2\pi}{M}. \end{cases} \tag{4.12}$$

Please cite this article in press as: Griffiths LS, Porter R. Focusing of surface waves by variable bathymetry. Applied Ocean Research (2011), doi:10.1016/j.apor.2011.08.004

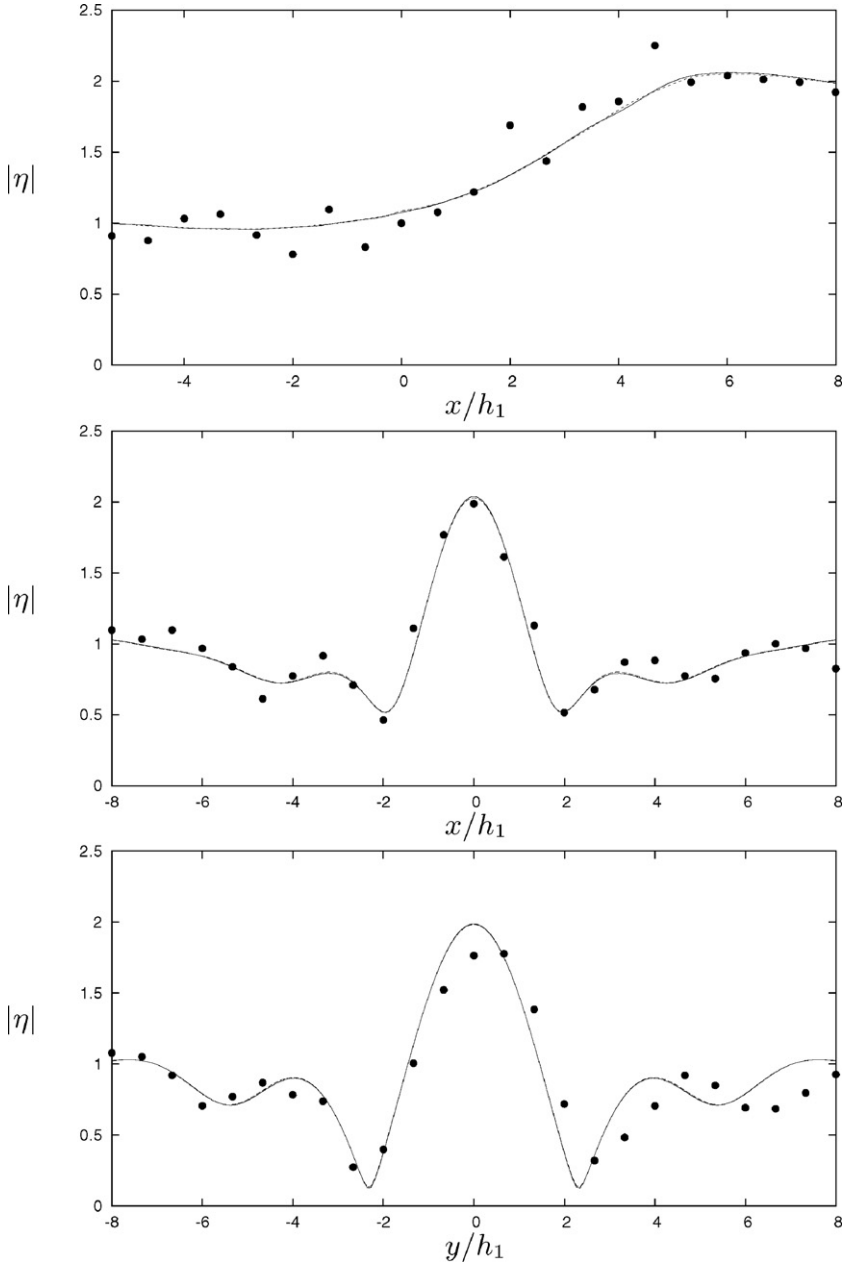

Fig. 3. Comparison of maximum wave amplitudes with experimental measurements of [11] for a circular shoaling domain with parabolic height profile along sections $y = 0$, $x/h_1 = 5.3333x/h_1 = 8$.

As before, we need to calculate the contribution from the singular part of the Greens function, which is given in this context by

$$G^s_{ij}(r', \theta') = \frac{1}{4\pi} \iint_{D_{ij}} \ln(k_1^2(r^2 + r'^2 - 2rr' \cos(\theta - \theta')))r \, \mathrm{d}r \, \mathrm{d}\theta. \tag{4.13}$$

Here, integration over domain variables r and θ cannot both be done analytically as in the Cartesian case and, after integrating with respect to r, we are left with

$$G^s_{ij}(r', \theta') \approx \frac{r_i}{4\pi} \int_{\theta_j - (1/2)\Delta_\theta}^{\theta_j + (1/2)\Delta_\theta} \Big[r \ln(k_1^2(r^2 + \sigma^2)) - 2r + 2\sigma \tan^{-1}\left(\frac{r}{\sigma}\right) \Big]_{r_l}^{r_u} \mathrm{d}\theta, \tag{4.14}$$

where $\sigma = r' \sin(\theta - \theta')$, $r_u = r_i + (1/2)\Delta_r - r' \cos(\theta - \theta')$ and $r_l = r_i - (1/2)\Delta_r - r' \cos(\theta - \theta')$ which must be calculated numerically. Then the analogue of (4.5) is

$$\psi(r', \theta') + \sum_{i=1}^{N} \sum_{j=1}^{M} a_{ij} [\kappa(r_i, \theta_j) - k_1^2] \{ r_i \Delta_r \Delta_\theta G_b(r_i, \theta_j; r', \theta') + G^s_{ij}(r', \theta') \} = \psi_{inc}(r', \theta'; \beta), \tag{4.15}$$

where the coefficients a_{ij} satisfy

$$a_{pq} + \sum_{i=1}^{N} \sum_{j=1}^{M} a_{ij} [\kappa(r_i, \theta_j) - k_1^2] \{ r_i \Delta_r \Delta_\theta G_b(r_i, \theta_j; r_p, \theta_q) + G^s_{ij}(r_p, \theta_q) \} = \psi_{inc}(r_p, \theta_q; \beta), \tag{4.16}$$

for $q = 1, \ldots, N$, $p = 1, \ldots, M$. Note that here, in polars, we may write $\psi_{inc}(r, \theta; \beta) = \mathrm{e}^{\mathrm{i}k_1 r \cos(\theta - \beta)}$.

Please cite this article in press as: Griffiths LS, Porter R. Focusing of surface waves by variable bathymetry. Applied Ocean Research (2011), doi:10.1016/j.apor.2011.08.004

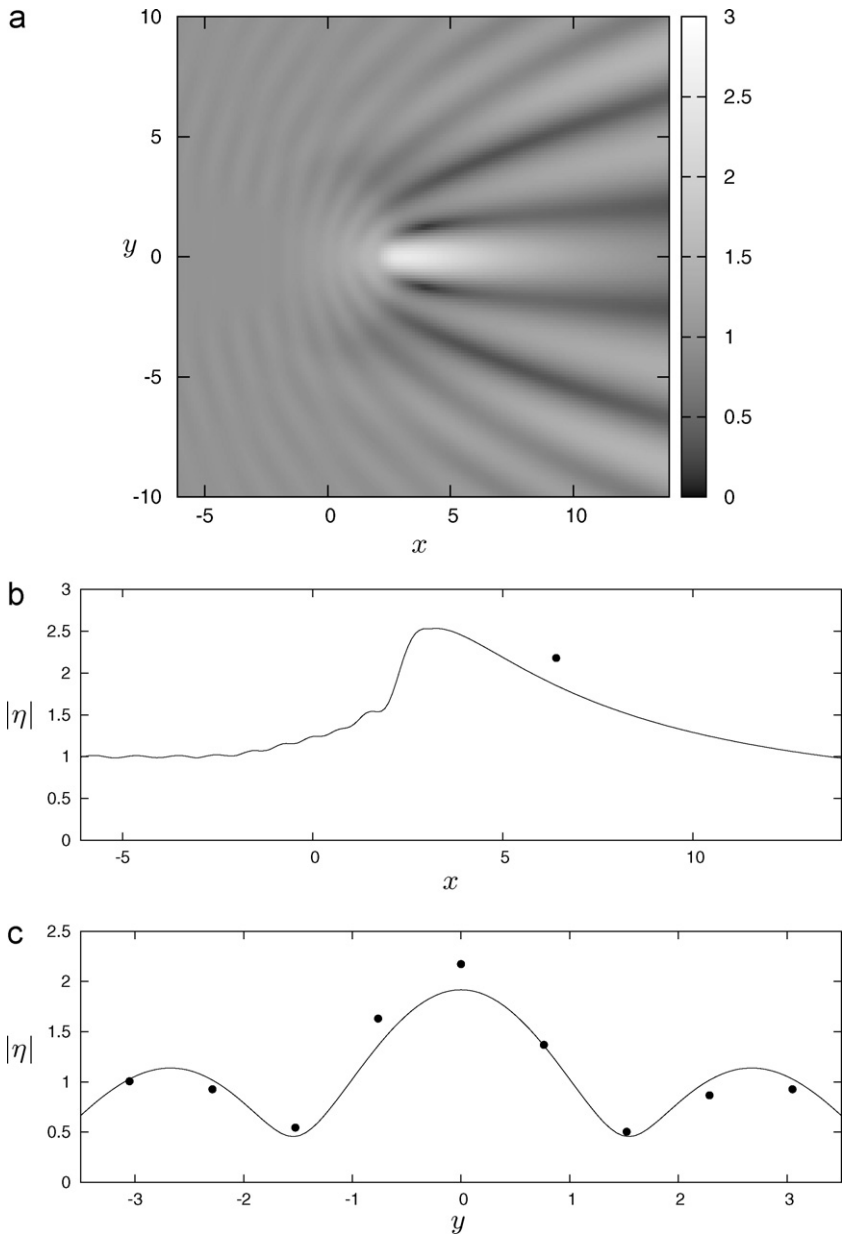

Fig. 4. The geometry of [29] for an ellipsoidal bed protrusion centred at (0, 0): (a) a surface plot of $|\eta|$; (b) $|\eta|$ along $y=0$; (c) $|\eta|$ along $x=6.1$ m. The circular dots represent the experimental M2 results of [29].

Subsequently, the scattering amplitude may be computed from a minor adaptation of (4.7) to give

$$\mathcal{A}(\theta';\beta)=\frac{1}{4}\mathrm{i}\Delta_r\Delta_\theta\sum_{i=1}^{N}\sum_{j=1}^{M}r_i a_{ij}[\kappa(r_i,\theta_j)-k_1^2]\psi_{inc}(r_i,\theta_j;\pi+\theta'). \tag{4.17}$$

4.3. Bathymetry with symmetry

Computational savings can be made if the bathymetry $z=h(x, y)$ has a plane of symmetry, say along $y=0$. Then the original boundary-value problem can be decomposed into its symmetric and antisymmetric components, by first writing

$$\psi_{inc}=\frac{1}{2}\left(\psi^s_{inc}+\psi^a_{inc}\right), \tag{4.18}$$

where

$$\psi^{s,a}_{inc}=\left(\psi_{inc}(x,y;\beta)\pm\psi_{inc}(x,y;-\beta)\right), \tag{4.19}$$

such that $\partial_y\psi^s_{inc}=0$ on $y=0$ and $\psi^a_{inc}=0$ on $y=0$. The forcing from each component implies a response satisfying the same symmetry conditions on $y=0$, and thus we decompose the total potential ψ similarly into symmetric and antisymmetric components,

$$\psi=\frac{1}{2}\left(\psi^s+\psi^a\right), \quad \text{such that } \partial_y\psi^s(x,0)=0,\ \psi^a(x,0)=0, \tag{4.20}$$

and the problems for $\psi^{s,a}$ can be solved in the half-plane $y>0$ with the boundary conditions (4.20) in place and the relations $\psi^{s,a}(x,-y)=\pm\psi^{s,a}(x,y)$ providing the extension to the lower-half plane.

Please cite this article in press as: Griffiths LS, Porter R. Focusing of surface waves by variable bathymetry. Applied Ocean Research (2011), doi:10.1016/j.apor.2011.08.004

It follows that the scattering coefficients $\mathcal{A}^{s,a}(\theta;\beta)$ defined by the solutions of these two problems, can be used to determine the overall scattering coefficient using

$$\mathcal{A} = \frac{1}{2}\left(\mathcal{A}^s + \mathcal{A}^a\right), \tag{4.21}$$

where

$$\psi^{s,a} \sim \mathcal{A}^{s,a}(\theta;\beta)\left(\frac{2}{\pi k_1 r}\right)^{1/2} \mathrm{e}^{\mathrm{i}k_1 r - \mathrm{i}\pi/4}, \quad k_1 r \to \infty, \tag{4.22}$$

remains in place.

The change to the method of solution requires that the Greens function be adapted in each symmetry to reflect the particular boundary condition (4.20) imposed on $\psi^{s,a}$. Thus we simply define

$$G^{s,a}(x,y;x',y') = -\frac{\mathrm{i}}{4}\left(H_0(k_1\rho) \pm H_0(k_1\hat{\rho})\right), \tag{4.23}$$

where $\hat{\rho}^2 = (x-x')^2 + (y+y')^2$, and the additional term is due to an image source about the line $y=0$. We treat the singular parts of each component of $G^{s,a}$ analytically as outlined in (4.6) or (4.14) in the case of a circular domain. The numerical discretisation now has to be performed only over the domain $y \geq 0$ and so, for the same numerical accuracy, the size of the linear systems of equation is halved and little extra cost in terms of computing the matrix coefficients.

Clearly, if $x=0$ and $y=0$ are both planes of geometric symmetry, we may decompose the problem further and define a sub-problem over one quadrant of the original domain.

5. Results

5.1. Validation

A series of tests of convergence have been performed on the numerical method on a generic bed profile given by

$$h = h_1 - \frac{1}{4}h_{max}\left(1+\cos\left(\frac{\pi x}{a}\right)\right)\left(1+\cos\left(\frac{\pi y}{b}\right)\right), \quad -a < x < a, -b < y < b, \tag{5.1}$$

where h_{max} is the maximum height above h_1 of the undulation. The method of Section 4.3 is used to exploit the $y=0$ plane of symmetry in this example and later ones also. With $\beta=0$, $h_{max}/h_1 = 1/2$, $a/h_1 = b/h_1 = 20$ and $k_1 h_1 = 1$, Table 1 shows computations of two measures of error in the solution, one a 'near-field' measure and the other a 'far-field' measure, and both functions of increasing numerical discretisation parameter N. We have taken $M = N/2$, in these calculations when symmetry is being used to discretise half of a square domain. Errors are measured relative to the solution computed with $N=192$, as there are no exact solutions to compare with. The root mean squared error in the maximum amplitude of the surface elevation is computed by sampling surface amplitudes on a regular 100 by 100 grid over the undulating domain. The error in the total circular wave scattered energy, $\mathcal{E}$ defined by (3.34), is measured relative to $N=192$. Similar results are shown in Table 2 for the same wavelength, $\lambda/h_1 = 2\pi$, relative to the depth at infinity, but over a larger domain defined by $a/h_1 = b/h_1 = 40$. A careful analysis of the results from convergence test suggest that the error reduces roughly like $O(1/N^2)$. Using the numerical data and assuming a $1/N^2$ decay extrapolated to $N=\infty$ suggests that an error of less than 1% can be obtained if the truncation parameter N is chosen so that at least 12 grid points per wavelength is achieved, or $\lambda/\min(\Delta_x, \Delta_y) \geq 12$. For such a low resolution of the wave field, this is an impressive result given the course numerical scheme used. The computational cost associated with this numerical method is high, requiring the inversion of a $NM \times NM$ complex-valued matrix (the evaluation of the matrix elements is quick compared to inversion), and so very short wavelength/large domain computations become prohibitively processor and storage expensive.

Table 1
Two error measures as a function of truncation parameter for a double-cosine bed profile: $a/h_1 = b/h_1 = 20$, $\lambda/h_1 = 2\pi$.

N	RMS error in $\lvert\eta\rvert$ relative to $N=192$	Error in $\mathcal{E}$ relative to $N=192$
24	0.02655	0.00065
48	0.00740	0.01476
72	0.00319	0.00683
96	0.00159	0.00349
120	0.00083	0.00184
144	0.00042	0.00092
168	0.00016	0.00036

Fig. 2(a) and (b) shows the instantaneous free surface and the maximum free surface amplitudes for the parameters corresponding to Table 2. It can be seen that roughly 6 wavelengths cross the undulating part of the bed and that there is some focusing behind the raised double-cosine bed profile, which can be explained by refraction from the two sloping sides of the raised bed.

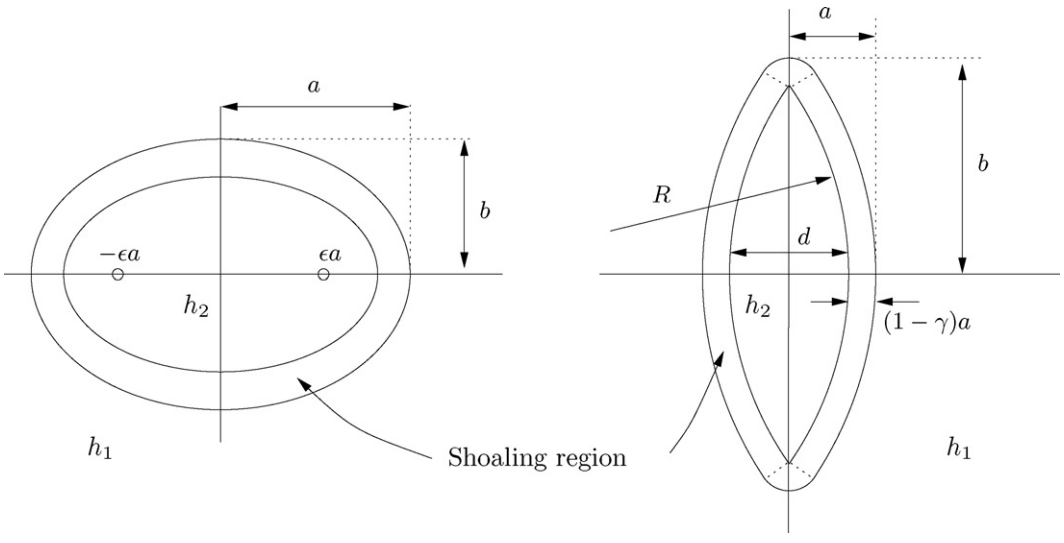

Fig. 5. Geometric specification of the two lenses in plan view.

Please cite this article in press as: Griffiths LS, Porter R. Focusing of surface waves by variable bathymetry. Applied Ocean Research (2011), doi:10.1016/j.apor.2011.08.004

Table 2
Two error measures as a function of truncation parameter for a double-cosine bed profile: $a/h_1 = b/h_1 = 40$, $\lambda/h_1 = 2\pi$.

N	RMS error in $\|\eta\|$ relative to $N = 192$	Error in $\mathcal{E}$ relative to $N = 192$
24	0.37382	0.09998
48	0.02589	0.00339
72	0.01207	0.01228
96	0.00636	0.00804
120	0.00364	0.00469
144	0.00187	0.00248
168	0.00075	0.00101

The method has also been applied to a circular shoaling domain with a parabolic height profile given by

$$h(r,\theta) = h_1 - h_{max}\left(1 - \frac{r^2}{b^2}\right), \quad r \le b,$$

which has been used by [15,14,21] to compare against experimental data from [11]. This bed profile which again has a peak height of h_{max} above h_1 has non-vanishing gradient on the boundary $r = b$ where $h_r(b,\theta) = 2h_{max}/b$ and so we are required to include the additional contribution from the boundary integral (3.32), (3.34), (3.37) into our method. This is relatively straightforward for a boundary which is aligned with a circular grid, the approximated additional contribution to the left-hand side of the discretised system (4.16) being given by

$$A(h_1)\sum_{j=1}^{M} a_{Nj} h_r(b,\theta_j)(b\Delta_\theta G_b(b,\theta_j;r_p,\theta_q) + \tilde{G}_j^s(r_p,\theta_q)),$$

where

$$\tilde{G}_j^s(r',\theta') = \frac{1}{4\pi}\int_{\theta_i-\theta'-(1/2)\Delta_\theta}^{\theta_i-\theta'+(1/2)\Delta_\theta} \ln(k_1(b^2 + r'^2 - 2br'\cos t))\,\mathrm{d}t,$$

is evaluated numerically.

Results are displayed in Fig. 3. The experimental parameters used by [11] are $h_1 = 0.15$ m, $h_{max} = 0.1$ m (so that the water depth above the peak of the shoal is 0.05 m), $b = 0.8$ m with an incident wavelength of 0.4 m and waveangle of $\beta = 0$. This gives $k_1 h_1 = 2.3561$, $b/h_1 = 5.333$. The three panels in Fig. 3 show the maximum wave amplitude (normalised by the incident wave amplitude), defined by (3.33) along the sections $y = 0$, $x = b$ (the rear of the shoal) and $x = (3/2)b$. The circles show the experimental results of [11] and each panel includes three almost indistinguishable lines; two solid curves overlay one another almost exactly are computed using Cartesian and circular grids but do not include the additional contribution from the slope discontinuity along the edge of the shoal. The dashed curve which deviates slightly from these two curves represents the inclusion of the additional term from the bed discontinuity in the computation based on a circular grid. These curves appear to be a significant improvement in fig. 2 of [14] and compare favourably with those shown in [21] although there are some small qualitative differences especially between our Fig. 3 and figure 11 in [21].

We remark that although the additional contribution from the boundary integral along the bed slope discontinuity makes a practically insignificant difference to the results shown in Fig. 3, its omission in other more severe discontinuities could be important (see, for example, fig. 12 of [21]).

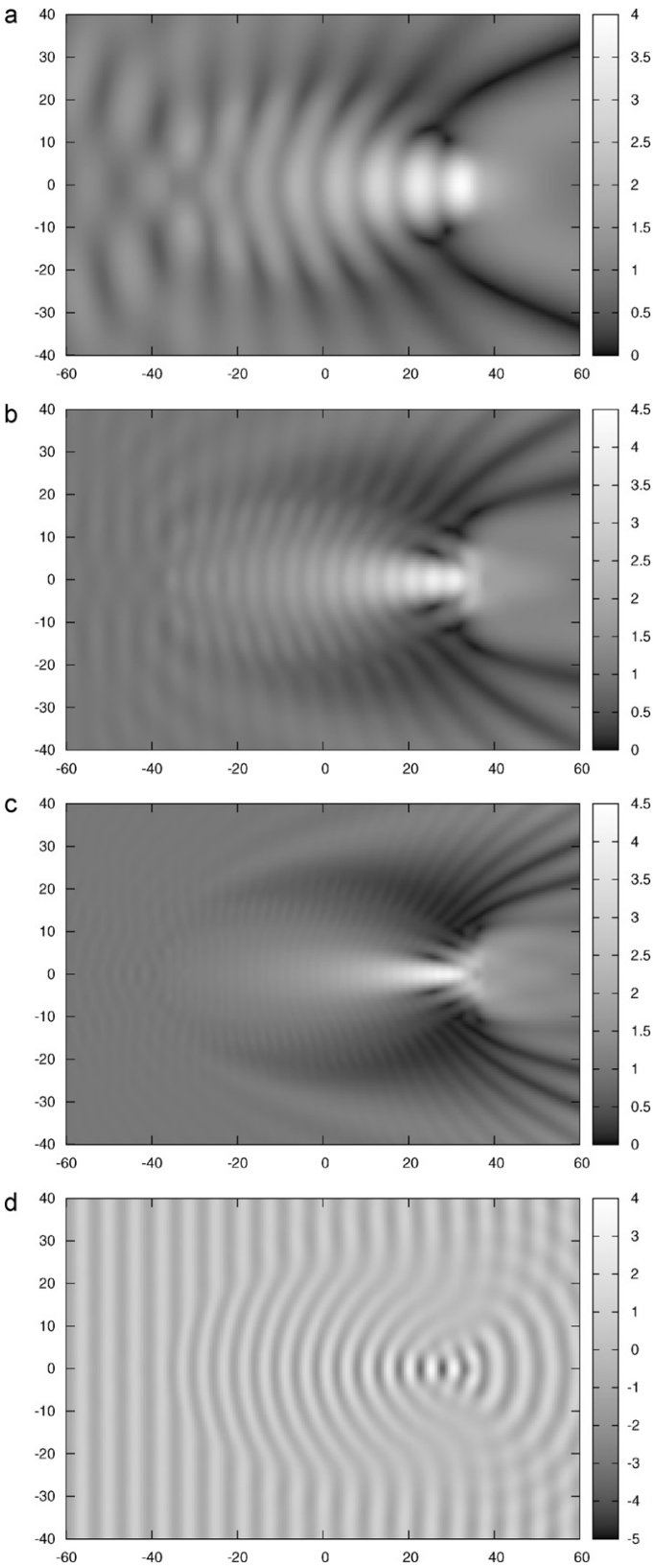

Fig. 6. In (a)–(c), the maximum free surface displacement $|\eta|$ is shown for focusing by an elliptical lens for $a/h_1 = 40$, $\beta = 0$, $\gamma = 0.8$, and $h_2/h_1 = 1/2$ with: (a) $k_1 h_1 = 1/4$, $b/h_1 = 28.0$; (b) $k_1 h_1 = 1/2$, $b/h_1 = 27.7$; (c) $k_1 h_1 = 1$, $b/h_1 = 26.05$ in (c). In (d), the instantaneous free surface corresponding to (c) is shown.

Please cite this article in press as: Griffiths LS, Porter R. Focusing of surface waves by variable bathymetry. Applied Ocean Research (2011), doi:10.1016/j.apor.2011.08.004

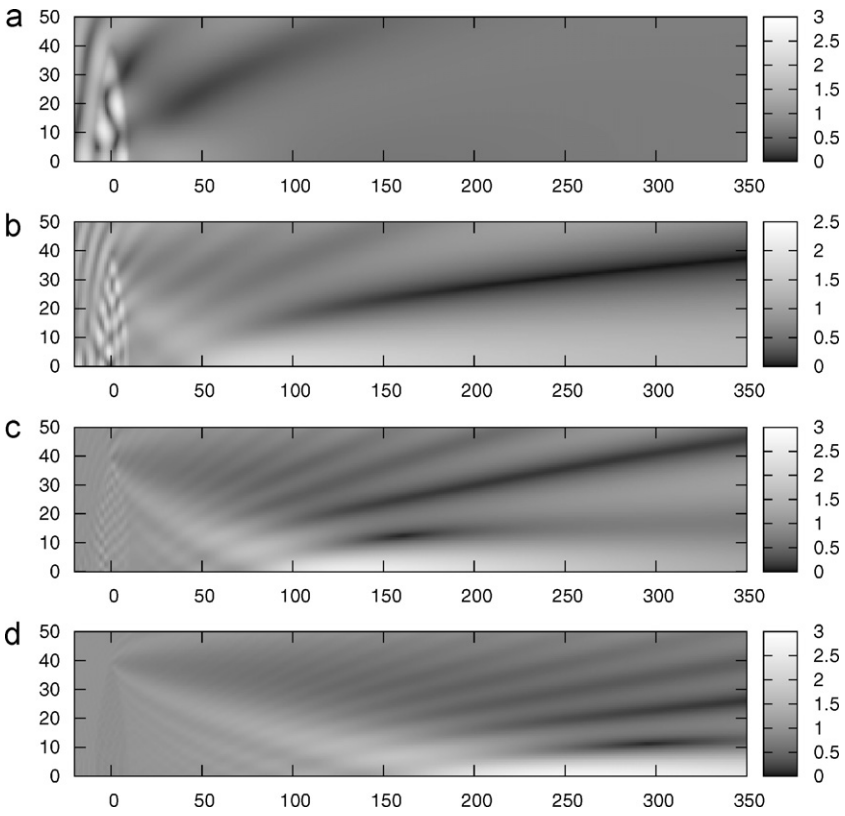

Fig. 7. Maximum free surface displacement $|\eta|$ for focusing by a bi-convex lens with $a/h_1 = 10$, $b/h_1 = 40$, $\beta = 0$, $\gamma = 0.8$, and $h_2/h_1 = 1/2$ with $k_1 h_1 = 1/4$ in (a), 1/2 in (b), 1 in (c) and 2 in (d).

As a final test of the method, we apply it to the ellipsoidal bed protrusion of [29], given by

$$\frac{h}{h_1} = 2 - \frac{5}{3}\left(1 - \left(\frac{x}{3.81}\right)^2 - \left(\frac{y}{4.95}\right)^2\right)^{1/2}, \quad \text{for} \quad \left(\frac{x}{3.05}\right)^2 + \left(\frac{y}{3.96}\right)^2 \le 1$$

(units of metres) with $h_1 = 0.4572$ m and maximum height $h_{max} = (2/3)h_1 = 0.3048$ m. The incident wave period is 1.3 s which translates to a non-dimensional wavenumber of $k_1 h_1 = 1.273$ whilst $\beta = 0$.

Fig. 4(a) illustrates the amplification of waves behind the ellipsoidal protrusion in a surface plot whilst Fig. 4(b) and (c) shows the surface elevation along the centreline, $y = 0$, of the geometry and along 'transect 4' of [29] at $x = 6.1$ m in our results where the bed protrusion is centred on (0, 0). There is good agreement with the experimental monochromatic M2 measurements of [29] and favourable agreement with the more accurate 'FUNWAVE' set of results of [8] (figures 2 and 3) who used both a parabolic wave model which fails to account for reflective effects of the bed and FUNWAVE, a fully non-linear time-dependent Boussinesq model of wave propagation.

5.2. Elliptical lens

To describe the bathymetry used here, we employ elliptical coordinates (u, v) with $x = c\cosh u \cos v$, $y = c \sinh u \sin v$. Here $c = a\epsilon = \sqrt{a^2 - b^2}$ (with $a > b$) is the distance of the foci from the origin defined so that the ellipse $u = u_0$ with $u_0 = \cosh^{-1}(a/c)$ touches the sides of the rectangular domain $D_{ab} := \{-a < x < a, -b < y < b\}$ – see Fig. 5. Then we define $h(x, y) \equiv h(u, v)$ by

$$hh = \begin{cases} h_2, & u < u_1 \\ h_1 - \frac{1}{2}(h_1 - h_2)\left(1 + \cos\left(\frac{\pi(u - u_1)}{u_0 - u_1}\right)\right), & u_1 < u < u_0, \end{cases} \tag{5.2}$$

where $u_1 = \gamma u_0$ (these definitions are not related to those used briefly in (3.12)) and γ controls the distance over which shoaling from the depth h_1 to the depth of the plateau h_2 occurs. Typically, we have taken $\gamma = 0.8$ so that roughly 80% of the undulating bed is occupied by a flat elliptical plateau of height $h_{max} = h_1 - h_2$ and 20% is reserved for shoaling. The depth function h is used to define κ in (3.19), and for this standard results in elliptical coordinates for the gradient and Laplacian can be used.

Fig. 6 illustrates focusing over an elliptical lens which has its length a/h_1 fixed at 40, the height of the elliptical plateau, h_2, set at half the depth of the fluid outside the lens and the shoaling parameter γ set at 0.8. These results are typical of numerical experiments with other parameters and exhibit the key features of those results. In panels (a)–(c), we plot the maximum amplitude, $|\eta|$, of the total wave field over a domain including the elliptical lens as the wavenumber increases from $k_1 h_1 = 1/4$ through 1/2 to a value of 1. Corresponding wavelengths range from $8\pi h_1$ to $2\pi h_1$ representing a varying bed which is between three to twelve wavelengths long. This indicates the numerical parameters needed to discretise the domain according to the rules established in the previous section. The ray theory result in (2.1) is used to determine the ellipticity, ϵ, for focusing and this defines b/h_1 for each value of $k_1 h_1$, given in the caption to Fig. 6. The results clearly indicate an increases focusing effect towards the far focal point of the ellipse (which varies according to the value of ϵ used, but is roughly centred at $x/h_1 = 30$). In particular, notice in Fig. 6(c) the shadow region formed in the hind quarters of the elliptical domain due to the incident waves

Please cite this article in press as: Griffiths LS, Porter R. Focusing of surface waves by variable bathymetry. Applied Ocean Research (2011), doi:10.1016/j.apor.2011.08.004

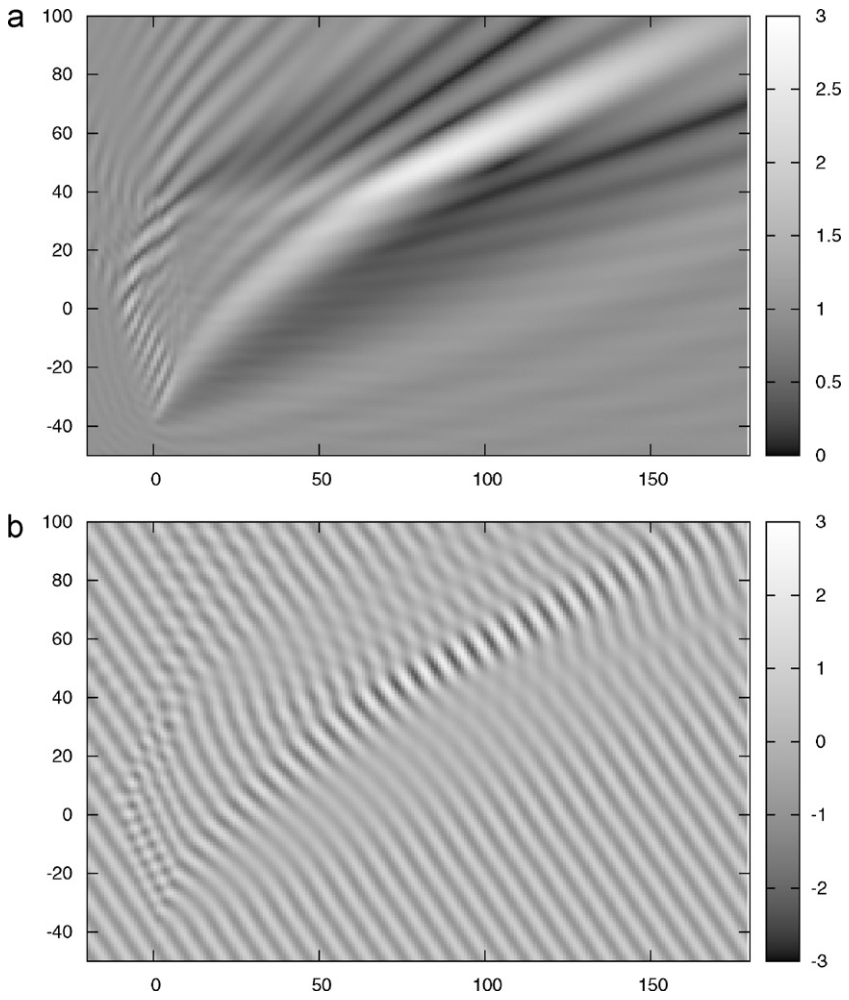

Fig. 8. Maximum free surface displacement $|\eta|$ and instantaneous surface for a bi-convex lens with $a/h_1 = 10$, $b/h_1 = 40$ and $h_2/h_1 = 1/2$, $k_1 h_1 = 1$ and with oblique wave incidence of $\beta = \pi/6$.

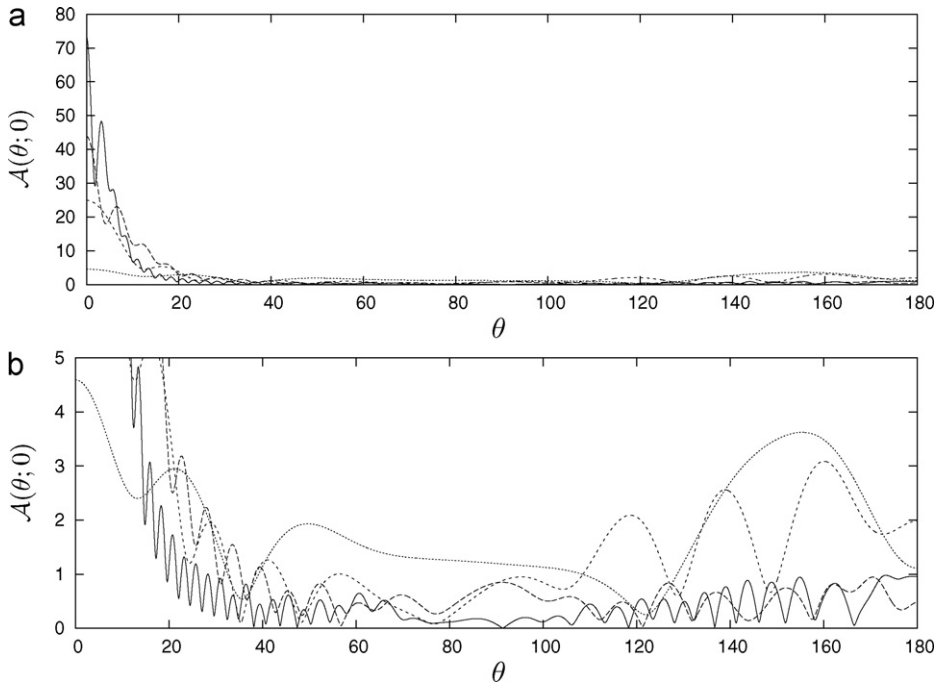

Fig. 9. The diffraction coefficient $\mathcal{A}(\theta;0)$ a bi-convex lens with $a/h_1 = 10$, $b/h_1 = 40$, $\beta = 0$, $\gamma = 0.8$, and $h_2/h_1 = 1/2$ with $k_1 h_1 = 1/4$ (dot dash), 1/2 (dotted), 1 (dashed) and 2 (solid). Detail shown in (b).

Please cite this article in press as: Griffiths LS, Porter R. Focusing of surface waves by variable bathymetry. Applied Ocean Research (2011), doi:10.1016/j.apor.2011.08.004

Table 3
Computational results for focal lengths and amplitudes compared against predictions from ray theory.

k_1h_1	n	Predicted f/h_1	Measured f/h_1	$\|\eta\|$ at focus
1/4	1.407	118	33	1.21
1/2	1.386	124	90	1.82
1	1.318	151	135	2.63
2	1.169	280	259	2.76

having being bent round towards the focal point. Notice also how the short wavelength results feature only a small diffracted wave component; mostly the waves are being refracted by the varying bed in this limit.

In Fig. 6(d) we also plot the instantaneous free surface amplitude which shows quite clearly the bending of the incident wave front and the focal point.

5.3. Convex lens

The description of the bathymetry for a bi-convex lens is complicated by the need for a smoothly varying shoaling region connecting a bi-convex lens shaped plateau of depth h_2 with the constant depth h_1. As in the previous example, we use a parameter γ to control what proportion of the undulating bed is used for shoaling and design the bed to fit within a rectangular domain, D_{ab}. See Fig. 5 for reference. The radius of curvature of the bi-convex lens is defined by R, as in (2.2), and given by the solution of

$$R^2 = (b-(1-\gamma)a)^2 + (R-\gamma a)^2. \tag{5.3}$$

The region $y^2+(R-\gamma a+|x|)^2 < R^2$, defines the plateau in which $h=h_2$. When $R<r_1<R_1$, where $r_1 = (y^2+(R-\gamma a+|x|)^2)^{1/2}$ and $R_1=(R+(1-\gamma)a)$ with $|y|/(R-\gamma a+|x|) < (b-(1-\gamma)a)/(R-\gamma a)$, the shoaling sides of the bed are defined by

$$h = h_1 - \frac{1}{2}(h_1-h_2)\left(1+\cos\left(\frac{\pi(r_1-R)}{R_1-R}\right)\right). \tag{5.4}$$

Finally, when $r_2<R_2$ where $r_2 = (x^2+(|y|-b+(1-\gamma)a)^2)^{1/2}$, and $R_2=(1-\gamma)a$ with $|y|/(R-\gamma a+|x|) > (b-(1-\gamma)a)/(R-\gamma a)$ then the shoaling sections at the ends of the lenses are defined by

$$h = h_1 - \frac{1}{2}(h_1-h_2)\left(1+\cos\left(\frac{\pi r_2}{R_2}\right)\right). \tag{5.5}$$

Outside of these three regions, which connect smoothly with each other, the depth is h_1. Here $|\nabla h|^2 = h_r^2$ and $\nabla^2 h = h_{rr}+(1/r)h_r$ according to the particular definition of r (r_1 or r_2) being used.

A value of $\gamma=0.8$ has been used for the results presented here. For comparison with (2.2), the width of the lens is $d=2\gamma a$.

Fig. 7 shows a series of computed maximum free surface amplitudes for a fixed bi-convex lens geometry as the wavenumber, k_1h_1, increases. As k_1h_1 increases, then so the wavelength decreases and, since the ratio h_2/h_1 is fixed (at a half), the refractive index changes (see Table 3) thus lengthing the focal distance of the lens. It is clear that waves become more focussed as the wavelength shortens and the refractive effects of the lens become increasingly dominant over diffractive effects.

Table 3 shows how numerical results illustrated in Fig. 7 compare with predictions from using the ray theory result, (2.2) and indicate a closer agreement with ray theory for shorter wavelengths. There is a small percentage difference between the measured and predicted focal distances, but this may be because of the shoaling from the bed to the plateau distorting ray paths as described in the Introduction.

In Fig. 9, the scattered wave amplitude $\mathcal{A}(\theta;0)$ is shown against θ between zero and 180° for the series of numerical experiments in Fig. 7. It can be seen that as the wavelength is reduced, less diffraction is being produced and more wave energy is refracted in higher concentrations towards $\theta=0$.

Finally, we illustrate in Fig. 8 that focusing still occurs for short waves obliquely incident on the same geometry used in Fig. 7. Thus, the wave angle is $\beta=\pi/6$ and whilst ray theory does not predict perfect focusing for oblique angle of incidence, it does predict the formation of a cusp.

6. Conclusions

An integral equation formulation to the problem of surface wave scattering by a finite region of arbitrary undulating bathymetry has been presented. The assumptions of a smoothly varying bed have allowed us to use the modified mild-slope equations to vertically average the three-dimensional fluid motion. This formulation has been used to consider focusing of plane incident waves by two types of raised bathymetry, each motivated by ray-theory results for short wavelengths. Thus we have considered focusing by a raised elliptical plateau and by a raised bi-convex lens shaped plateau. The numerical scheme used for computing solutions is basic but easy to implement and we have outlined two types of discretisation based on circular and rectangular domains. Although the numerical cost is high as the numerical scheme is refined, results have suggested good accuracy even with relatively course discretisations. We have shown that elliptical lenses can be much more effective at focusing than conventional bi-convex lenses in the context of refraction of surface waves by raised bathymetry. Although the elliptical lens requires a larger raised area than a bi-convex lens, the geometry of [13] which we have not explored here should exhibit the same focusing effects as the elliptical lens but which a much smaller area of raised bed.

Focusing of wave energy may be a useful way of increasing energy capture by wave energy converters placed in the ocean especially if used in moderate wave environments. For example, in the convex lens example, waves of different frequencies focus at different distances behind the lens and hence converters tuned to different frequencies could be placed at the appropriate focal lengths behind a lens.

The method of scattering of surface waves by an finite domain of arbitrary slowly varying bathymetry has been applied here to focusing, but can be extended in a number of directions, such as interactions between multiple finite domains of varying bathymetry, near trapping by long finite ridges and edge wave excitation along semi-infinite ridges (see [27]). Other extensions may include shoaling domains on sloping beds, as considered by [6,4] using the Green's function derived by [3].

References

[1] Abramowitz MA, Stegun I, editors. Handbook of mathematical functions. New York: Dover; 1965.
[2] Athanassoulis G, Belibassakis K. A consistent coupled-mode theory for the propagation of small-amplitude water waves over variable bathymetry regions. J Fluid Mech 1999;389:275–301.
[3] Belibassakis K. The Green's function of the mild-slope equations: the case of a monotonic bed profile. Wave Motion 2000;32:339–61.
[4] Belibassakis K, Athanassoulis G, Gerostathis ThP. A coupled-mode model for the refraction–diffraction of linear waves over steep three-dimensional bathymetry. Appl Ocean Res 2001;23:319–36.
[5] Berkhoff JCW. Computation of combined refraction–diffraction. In: Proc. 13th Intl Conf. on Coastal Engng., July 1972. Canada: Vancouver; 1973. p. 471–90.
[6] Berkhoff JCW, Booy WN, Radder AC. Verification of numerical wave propagation models for simple harmonic linear water waves. Coastal Eng 1982;6(3):255–79.
[7] Chamberlain PG, Porter D. The modified mild-slope equation. J Fluid Mech 1995;291:393–407.
[8] Choi J, Lim CH, Lee JI, Yoon SB. Evolution of waves and currents over a submerged laboratory shoal. Coastal Eng 2009;56(3):213–97.
[9] Hecht E. Optics. Addison Wesley Longman, Inc.; 1998.

Please cite this article in press as: Griffiths LS, Porter R. Focusing of surface waves by variable bathymetry. Applied Ocean Research (2011), doi:10.1016/j.apor.2011.08.004

[10] Hu X, Chan CT. Refraction of water waves by periodic cylinder arrays. Phys Rev Lett 2005;95:154501.
[11] Ito T, Tanimoto A. A method of numerical analysis of wave propagation – application to wave diffraction and refraction. In: Int. Conf. on Coastal Eng. 1972. p. 503–22.
[12] Kim J, Bai K. A new complementary mild-slope equation. J Fluid Mech 2004;511:25–40.
[13] Kudo K, Tsuzuku T, Iwai K, Akiyama Y. Wave focusing by a submerged plate. In: OCEANS'88. 'A partnership of marine interests'. Proceedings. 1988. p. 1061–6.
[14] Li B, Reeve DM, Fleming CA. Numerical solution of the elliptic mild-slope equation for irregular wave propagation. Ocean Eng 1993;20(1):85–100.
[15] Lo JM. A numerical method for combined refraction–diffraction of short waves on an island. Ocean Eng 1991;18(5):419–34.
[16] Maruo E. The drift force on a body floating in waves. J Ship Res 1960;4:1–10.
[17] Mehlum E, Stamnes J. On the focusing of ocean swells and its significance in power production. Cent. Inst. for Indust. Res., Blindern, Oslo, SI Rep. 77; 1978. p. 1–38.
[18] Mei CC. The applied dynamics of ocean surface waves. World Scientific; 1983.
[19] Mountford D. Refraction properties of conics. Math Gazette 1984;68: 134–7.
[20] Murashige S, Kinoshita T. An ideal wave focusing lens and its shape. Appl Ocean Res 1992;14:275–90.
[21] Naserizadeh R, Bingham HB, Noorzad A. A coupled boundary element-finite difference solution of the elliptic modified mild slope equation. Eng Anal Boundary Elem 2011;35:25–33.
[22] Porter D. The mild-slope equations. J Fluid Mech 2003;494:51–63.
[23] Porter R, Porter D. Interaction of water waves with three-dimensional periodic topography. J Fluid Mech 2001;434:301–35.
[24] Porter D, Staziker DJ. Extensions of the mild-slope equation. J Fluid Mech 1995;300:367–82.
[25] Smith R, Sprinks T. The scattering of surface waves by a conical island. J Fluid Mech 1975;72:373–84.
[26] Stamnes JJ, Lovhaugen O, Spjelkavik B, Mei CC, Lo E, Yue DKP. Nonlinear focusing of surface waves by a lens – theory and experiment. J Fluid Mech 1983;135:71–94.
[27] Thompson I, Linton CM, Porter R. A new approximation method for scattering by long finite arrays. Q J Mech Appl Math 2008;61:333–52.
[28] Toledo Y, Agnon Y. A scalar form of the complementary mild-slope equation. J Fluid Mech 2010;656:407–16.
[29] Vincent CL, Briggs MJ. Refraction–diffraction of irregular waves over a mound. J Waterway Ports Coastal Ocean Eng 1989;115(2):269–84.
[30] Zhang S, Williams AN. Wave scattering by a submerged elliptical disk. J Waterway Ports Coastal Ocean Eng 1996;122:38–45.
[31] Zhu S-P. A new DRBEM model for wave diffraction and refraction. Eng Anal Boundary Elem 1993;12:261–74.

Please cite this article in press as: Griffiths LS, Porter R. Focusing of surface waves by variable bathymetry. Applied Ocean Research (2011), doi:10.1016/j.apor.2011.08.004